



Enhancing Scan-to-BIM in Bridge Engineering through Point Cloud Completion

Tao Yang¹, Yang Zou¹, and Enrique del Rey Castillo¹

¹University of Auckland, Auckland, New Zealand
yang.zou@auckland.ac.nz

Abstract

Automatic generation of Building Information Models (BIMs) from point clouds (i.e., Scan-to-BIM) plays a critical role in bridge maintenance and the development of Digital Twinning (DT). However, the problem of incomplete point cloud (e.g., caused by occlusions in laser scanning) significantly hinders the Scan-to-BIM accuracy. To overcome this challenge, we propose addressing the occlusion problems in bridge point clouds by introducing an additional point cloud completion task in the Scan-to-BIM process. This new task aims to take incomplete bridge point clouds, following segmentation, as input, and generate complete point clouds as output. The learning-based completion model, Point Completion Network (PCN), is adopted to validate the proposed strategy and show robust completion performance for bridge components with varying levels of occlusion. It can improve the average 11.94 Chamfer Distance (CD) and 11.05 F-score for coarse completion, 8.35 CD and 1.59 F-score for dense completion. This study contributes to Scan-to-BIM by refining the Scan-to-BIM framework in bridge engineering and defining a point cloud completion task to facilitate the development of bridge DT systems.

1 Introduction

Bridges are essential in the infrastructure system but often suffer serious health issues due to prolonged usage and environmental factors (American Society of Civil Engineers ASCE, 2021). However, traditional bridge inspection methods, such as human-labour-based data collection and paper-based data management, are always subjective and inefficient, which results in a pressing demand for efficient and smart bridge maintenance, management, and operation systems. In recent years, Building Information Modelling (BIM) has been introduced into bridge management. BIM provides a robust platform for improving traditional bridge management practices by offering a centralised digital environment for storing, visualising, and managing detailed bridge information. By integrating emerging photogrammetry techniques and Artificial Intelligence (AI), as-is condition data of bridges can be rapidly captured and analysed to enhance bridge monitoring and management

(Khudhair et al., 2021). In this regard, the Digital Twin (DT) was further proposed to form a more comprehensive and systematic framework for the whole life cycle management of bridges (Honghong et al., 2023; Pregnotato et al., 2022). The DT can replicate physical bridges into their virtual twin models in the operation and maintenance phase (O&M), constructing and updating them based on multiple data sources and adding new functions to simulate different operation scenarios (Honghong et al., 2023).

To build a bridge DT, it is critical to reconstruct a geometric and semantically rich BIM model, reflecting the as-is condition of bridges. The model can serve as the foundation for subsequent bridge DT applications, such as decision marking, real-time monitoring, and visualisation (Honghong et al., 2023). Obtaining the geometric information is often the first step for reconstructing a semantically rich BIM model, known as Geometric Digital Twin (gDT) (Brilakis, 2024). Various emerging reality capture tools, such as laser scanning and photogrammetry techniques, have been introduced to capture geometric information primarily through 3D point cloud data. The point cloud data can be used for constructing geometric BIM for bridges when BIM models are not generated from the design stage (Scan-to-BIM) (Bosché, 2010; Bosché et al., 2014). However, the reconstruction process is highly human-dependent, low-efficiency, and error-prone (Lu et al., 2019). Automating these tasks still remains a global challenge.

Due to the general absence of BIM models for most existing bridges, Scan-to-BIM research has attracted growing attention (Schönfelder et al., 2023). In recent years, extensive research has focused on the Scan-to-BIM of different bridge types, including RC girder bridges, steel girder bridges, masonry arch bridges, and truss bridges (Yang et al., 2024). However, most research focused on point cloud segmentation tasks, and the research on bridge geometric information reconstruction has not been fully investigated. Only a few studies focused on this topic (Justo et al., 2023; Lu & Brilakis, 2019; Mafipour & Vilgertshofer, 2023; Mehranfar et al., 2021; Walsh et al., 2013; Yan & Hajjar, 2022). The proposed methods are primarily for some sample slab-beam bridges, and the reconstruction quality is highly affected by point cloud quality problems, particularly occlusion (Zhao et al., 2023). Although some strategies were designed to address occlusion problems in their methods, the over-consideration of data quality problems in reconstruction workflow poses more limitations on the selection of reconstruction algorithm, resulting in poor generalizability. No prior research has specifically aimed to complete the missing regions in bridge point clouds.

To address this challenge, this paper defines a new point cloud completion task in the existing Scan-to-BIM framework, enhancing geometric BIM reconstruction in bridge engineering, as shown in Figure 1. This task will take incomplete bridge point clouds following segmentation as input and aim to generate complete point clouds as output. To validate the proposed strategy, the learning-based completion model, Point Completion Network (PCN), is introduced to recover the complete point cloud from raw incomplete input with a coarse-to-fine strategy.

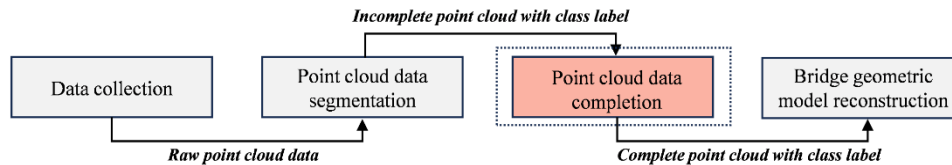


Figure 1: Role of point cloud completion in Scan-to-BIM

2 RELATED WORK

2.1 Geometric Digital Twinning of Bridges

Reconstructing 3D bridge geometric information from point clouds can be considered as a model-to-cloud fitting problem. To achieve this, the Constructive Solid Geometry (CSG) method was first adopted to generate the 3D model of bridge piers and pier caps (Walsh et al., 2013). A shape library containing generic objects (e.g., cuboid, cylinder) was established to fit the point cloud clusters. However, the CSG method relies highly on pre-defined geometrically simple solid primitives, which fail to capture complex bridge geometric information. After that, the Swept Solid Representation (SSR) based method was proposed to create a 3D shape by sweeping a 2D profile enclosed by a contour line along a specific path in 3D space. The bounding hulls, such as convex hulls (Preparata & Hong, 1977) and α -shape (Edelsbrunner & Mücke, 1994), are commonly adopted for 2D profile fitting. Lu and Brilakis (2019) proposed an object-fitting method to generate a gDT of existing RC bridges based on Industry Foundation Classes (IFC). The 2D ConcaveHull α -shape method was adopted for shape representation and parameter extraction, and four types of point clusters, including pier, pier cap, girder, and slab, are considered. Despite the satisfactory results, some point cloud quality problems, such as occlusion and uneven density, have been revealed to cause mismatch points and problems in concave hull generation.

An early model generation for steel girder bridges is proposed by Yan and Hajja (2022). The linear skeleton model was designed to extract the specific parameter value for 3D modelling. The scan information in data collection was utilised to improve the RANSAC-based parameter fitting, addressing the occlusion in model reconstruction. However, a pre-defined dummy model is required in the initial stages, which limits its ability to reconstruct other elements with different geometric features. Moreover, the parameter extraction accuracy relies heavily on the quality of occlusion labelling, and the significant occlusion remains a challenge in model reconstruction. To address occlusion issues, Mafipour and Vilgertshofer (2023) proposed a Parametric Prototype Model (PPM) to extract the parameters from segmented point clouds. The definition of different PPMs in the initial stage can enable the reliable parameter identification of bridge components and show satisfactory performance in sustaining occlusion. However, this method relies heavily on the PPM library, and prior knowledge and statistical study are required for parameter range setting. More importantly, the occlusion may not show much influence on the parameter extraction but will significantly affect the accurate selection of a PPM.

2.2 Learning-based Point Cloud Completion

The learning-based completion method is a promising solution for dealing with point cloud occlusion, arousing growing interest (Zhuang et al., 2024). The model can learn local and global features of incomplete input and output complete object shape and semantics. Research on learning-based completion methods can be classified into volumetric shape completion and point-wise completion according to different types of input data. However, translating the point cloud into 3D volume data would result in the loss of detailed geometric information, rendering it less generalisable for intricate shapes or 3D model construction with high LoD. Thus, many point-wise completion models have been proposed to generate complete shapes from given incomplete point clouds in recent years (Huang et al., 2020; Liu et al., 2020; Tchapmi et al., 2019; Wang et al., 2022; Wen et al., 2020; Yuan et al., 2018). The pioneer completion model, PCN, was proposed by Yuan et al. (2018), where an encoder-decoder architecture was adopted to complete the point cloud in a coarse-to-fine manner. After that, different improvements on the network were proposed to achieve better results, such as the feature-points-based completion network and multi-scale generating network in PF-Net (Huang et al.,

2020), the skip-attention mechanism in SA-Net (Wen et al., 2020), and multi-stages strategy in (Liu et al., 2020; Wang et al., 2022).

3 PROPOSED SOLUTION

This paper adopts raw PCN for bridge point cloud completion, addressing the occlusion problems in bridge point clouds prior to geometric reconstruction. The model is selected in this study for the following three reasons: (1) PCN is the classical and pioneering model for point cloud completion, with the most popular encoder-decoder network; (2) Despite being published in 2018, the completion performance still outperforms some newly published model in some shape types in the public dataset, e.g., plane, cabinet and car in ShapeNet (Yi et al., 2016); (3) Many completion models are limited to generating a fixed number of points e.g., 2048 or 4096 points. PCN is superior to some models by outputting dense point clouds through a coarse-to-fine strategy, significantly preserving the geometric features for BIM reconstruction.

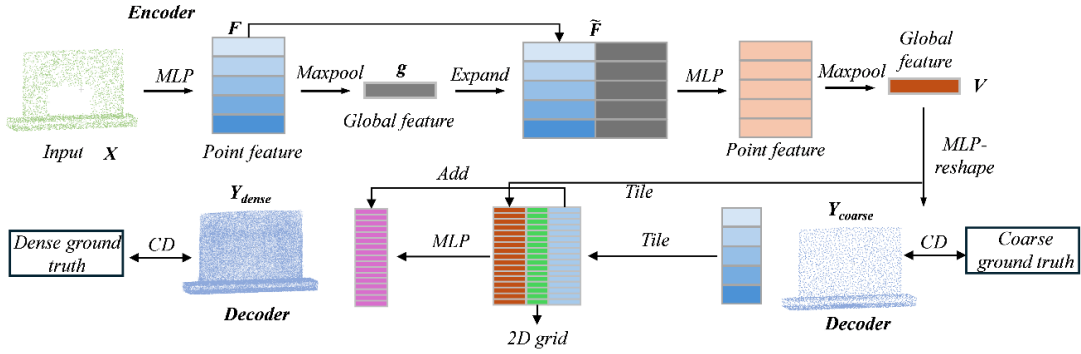


Figure 2: The architecture of the PCN model

As shown in Figure 2, PCN follows an encoder-decoder architecture. The encoder consists of two stacked PointNet (PN) layers. The input partial point cloud X is initially encoded into k -dimensional feature vector F through a multi-layer perceptron (MLP). A point-wise max-pooling operation is then applied to obtain k -dimensional global feature g . The second PN layer takes both g and F as inputs, outputting the augmented point feature \tilde{F} through feature concatenation. Finally, another MLP is adopted to generate the final global vector V .

The PCN adopts a multi-stage point generation process, starting from a coarse point cloud Y_{coarse} and progressing to dense point cloud Y_{dense} . A fully-connected decoder is utilised for coarse point cloud ($s \times 3$) generation, where the point number of coarse output s is set as 4096 points in this study. The generated output is compared with coarse ground truth data for loss calculations. After that, a folding-based operation is used to generate dense point clouds. In this step, a patch of t points is generated in the local area centred at each point P_i from Y_{coarse} and then transformed into the global coordinates by adding P_i to the output. The final result Y_{dense} consists of $n=st$ points, where the t is set as 4 and finally output 16384 points as dense output. Then, the loss is calculated between Y_{dense} and dense ground truth data. In this study, the symmetric version of Chamfer Distance (CD) is adopted to measure the difference between the output point cloud (Y_{out}) and the ground truth point cloud (Y_{GT}), as defined by Equation (1). Accordingly, the total loss for model training is defined by Equation (2).

$$L_{CD}(Y_{out}, Y_{GT}) = \frac{l}{|Y_{out}|} \sum_{p \in Y_{out}} \min_{q \in Y_{GT}} \|p-q\|_2^2 + \frac{l}{|Y_{GT}|} \sum_{q \in Y_{GT}} \min_{p \in Y_{out}} \|q-p\|_2^2 \quad (1)$$

$$L_{total}(Y_{coarse}, Y_{dense}, Y_{GT}) = L_{CD}(Y_{coarse}, \tilde{Y}_{GT}) + \alpha L_{CD}(Y_{dense}, Y_{GT}) \quad (2)$$

where the \tilde{Y}_{GT} and Y_{GT} are the ground truth of coarse point clouds and dense point clouds, respectively. α is the weight hyperparameter. The first term indicates the loss of coarse completion, and the second term represents the loss of dense completion. More details about the PCN model can be found in (Yuan et al., 2018), and the author's code can be accessed on GitHub (<https://github.com/wentaoyuan/pcn>).

4 EXPERIMENT AND RESULTS

This section details the results of the point cloud completion model for the validation of the proposed completion strategy. Three bridge components in the substructure are considered in this study, including piers, pier caps, and abutments, as shown in Figure 3. Commonly used types are selected for each component. The pier consists of circular piers, wall piers, and rectangular piers. Three types of pier caps are considered, as shown in Figure 3(d) to (f). Additionally, two typical abutment types are included, as shown in Figure 3(g) and (h).

To generate paired partial and completed point clouds, a series of 3D modes for each component type are generated beforehand. Each component was modelled as a Revit family, constrained by several design parameters, and then, C#-based Revit API was used to generate parametric models with varying design parameters automatically. Afterwards, the point clouds were generated from mesh sampling with a pre-defined point number set as 100000 points in this study. Voxel-based down-sampling is then performed to obtain dense complete point clouds (16384 points). The partial coarse point cloud is created by occlusion generation and down-sampling. Two different partial point clouds were generated from each complete point cloud, including the partial point clouds with a small occlusion and a large occlusion. The occlusion is created in three steps:

- Seed point selection: Random seed point selection from the point cloud.
- Radius calculation. This process begins by determining the coordinate range for X, Y, and Z, from which the maximum range is denoted as L . Then, the radius for small occlusion is calculated as $[0, 0.1L]$ and for large occlusion, as $[0.1L, 0.3L]$.
- Point removal. Once the seed point and radius are determined, points within the defined radius around the seed point are removed to generate the final partial point cloud.

Finally, the partial point clouds were uniformly down-sampled to 4096 points, providing the raw input for model training.

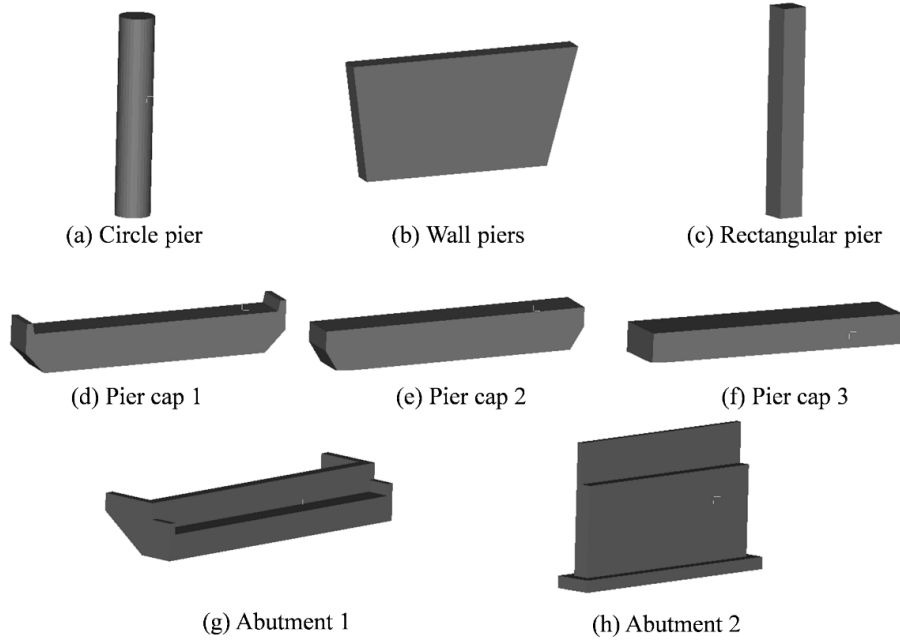


Figure 3: Component types in the training dataset

4.1 Implementation Details

The Pytorch framework was adopted for implementation on Ubuntu 22.04 through Intel® Xeon(R) Gold 6242R CPU and a single NVIDIA Quadro RTX 5000 GPU with 16 G memory. We trained the completion model for each bridge component to achieve the best completion performance. The dataset finally consists of 22500 piers, 25000 pier caps and 29000 abutments. The dataset was randomly split, with 90% used for training, 5% for validation, and the remaining 5% reserved for testing. Finally, the test and validation datasets contain 1200 pier instances, 1300 pier cap instances, and 1500 abutment instances, respectively. All our models were trained using the Adam optimiser with an initial learning rate of 0.0001 for 150 epochs and a batch size of 16. The learning rate decayed by 0.7 for every 50,000 iterations to fine-tune model performance.

4.2 Result and Evaluation

Point-wise metrics were employed to evaluate the performance of point cloud completion. The Chamfer Distance (CD) and F1-score were adopted for quantitative evaluation (Zhuang et al., 2024). The CD calculates the average closest distance between the output point cloud Y_{out} and the ground truth point cloud Y_{GT} , where the symmetric version of CD was used for comprehensive evaluation, as defined by Equation (1). The F-score, as shown in Equation (3), can assess the percentage of correctly reconstructed points according to pre-defined d , calculated by Precision (P) in Equation (4) and Recall (R) in Equation (5).

$$F\text{-Score}(d) = \frac{2P(d)R(d)}{P(d)+R(d)} \quad (3)$$

$$P(d) = \frac{I}{|X_{out}|} \sum_{p \in X_{out}} \left[\min_{q \in X_{GT}} \|q-p\| < d \right] \quad (4)$$

$$R(d) = \frac{1}{|X_{GT}|} \sum_{p \in X_{GT}} \left[\min_{q \in X_{out}} \|q-p\| < d \right] \quad (5)$$

The completion results of point clouds with large occlusion for abutments, pier caps, and piers are shown in Figures 4, 5, and 6, respectively. It can be observed that the PCN can effectively complete the occlusion in the raw point cloud, even with a significant loss of geometric information, outputting coarse results (4096 points) and dense results (16384 points). The prediction model can recover the missing point cloud from partial input and output the coarse results with clear boundary details. However, for dense results, some loss of detailed boundary geometric information can be found in these figures from the observation components boundary. Thus, while the PCN model can accurately predict the missing regions of the partial input using its fully connected decoder, the folding-based decoder for dense point cloud generation tends to result in a loss of boundary detail. This is because the folding-based decoder aims to predict approximating smooth surfaces, which limits its ability to recover sharp features along the component boundaries.

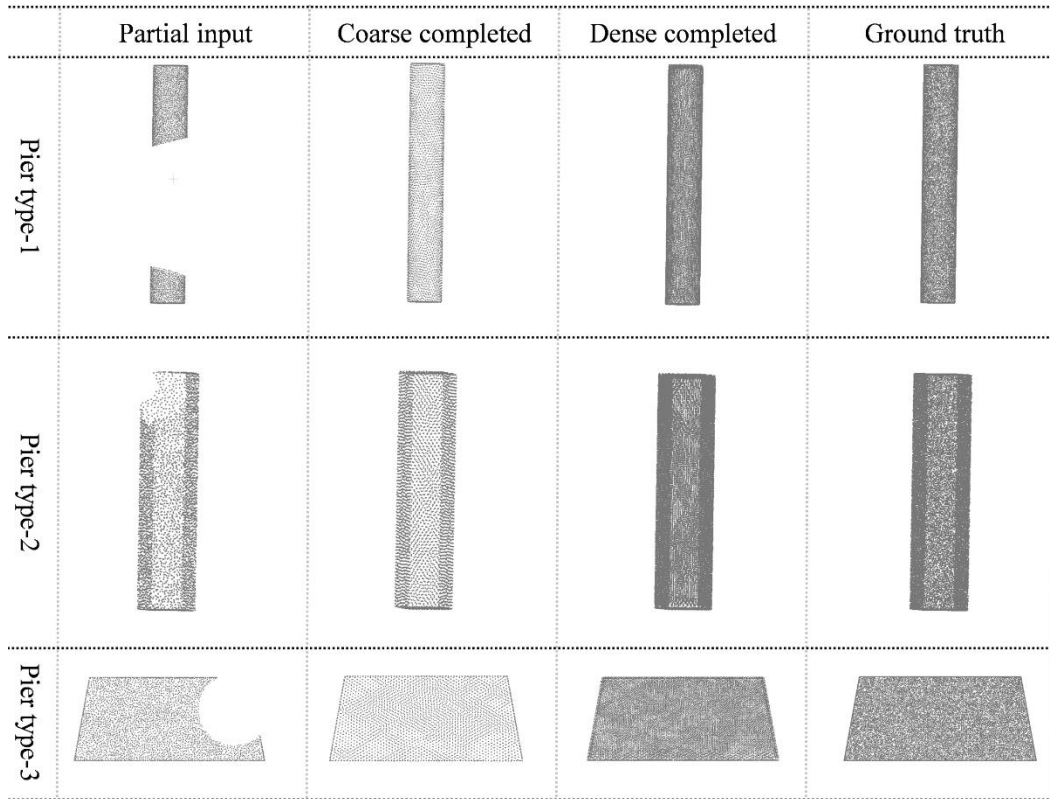


Figure 4: Completion results for piers


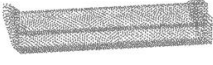


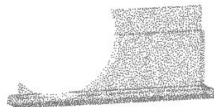
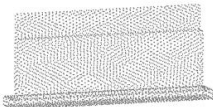
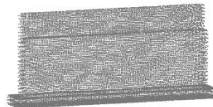
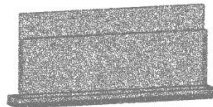
	Partial input	Coarse completed	Dense completed	Ground truth
Abutment - 1				
Abutment - 2				

Figure 5: Completion results for abutments






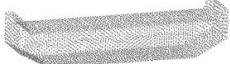



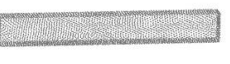


	Partial input	Coarse completed	Dense completed	Ground truth
Cap - 1				
Cap - 2				
Cap - 3				

Figure 6: Completion results for pier caps

Tables 1 and 2 provide the quantitative evaluation result for coarse and dense point cloud completion, respectively. Notably, the first row of each table compares the dense/coarse partial input with the corresponding dense/coarse ground truth, while the second row presents the calculation results for the dense/coarse ground truth and the recovered dense/coarse output from the partial input. The smaller CD values and large F-score values indicate better completion performance. For the F-score, different thresholds were set for different bridge components to effectively evaluate completion performance, as different bridge components have different scale sizes, resulting in different point cloud densities under a certain number of points. Accordingly, we set the thresholds of 0.05 m and 0.1 m for dense and coarse point cloud evaluation of piers and pier caps, while thresholds of 0.1 m and 0.2 m were applied for abutment completion evaluation.

These tables show that both results demonstrate a good performance in completing the bridge point cloud through PCN. The overall improvement of 11.94 CD and 11.05 F-score can be found for coarse completion, and 8.35 CD and 1.59 F-score can be found for dense results. Specifically, in the coarse output, improvements in CD of 16.97, 7.9, and 10.96 are achieved for abutment, pier, and pier cap, respectively, with corresponding F-score increases of 10.23, 7.94, and 14.97. For the dense output, CD reductions of 11.38, 4.47, and 9.22 are seen for abutment, pier, and pier cap, with F-score gains of 7.59, -8.09, and 5.29, respectively. The unsatisfactory result for pier completion may be attributed to the geometric loss in dense point cloud generation.

The detailed quantitative evaluation for point clouds with different scale occlusions is shown in Tables 3 and 4. Similarly, the PCN effectively mitigates occlusions in the bridge point cloud, as

reflected by the improved evaluation metrics. However, only slight CD improvements or even unsatisfactory results are observed for point cloud completion with smaller occlusions, highlighted in red. This diminished performance may be due to accuracy loss during the encoder-decoder process. Given the small radius, ranging from 0 to $0.1L$, for occlusion generation, the completion for minor occlusions does not yield noticeable improvements in evaluation metrics. At the same time, the accuracy loss in the encoder-decoder would be avoidable to deteriorate the evaluation results. From the observation in the F-score, despite the poor performance in CD, the point clouds become more complete according to the increased F-score. In contrast, the model significantly improves evaluation metrics for point clouds with larger occlusions despite the presence of accuracy loss.

Dataset	CD ($\times 10^2$)				F-score (%)			
	Abutment	Pier	Pier cap	Avg.	Abutment	Pier	Pier cap	Avg.
Partial input	37.67	19.39	22.34	26.46	87.16	85.92	80.29	84.45
After completion	20.70	11.49	11.38	14.52	97.39	93.86	95.26	95.50

Table 1: Overall evaluation of coarse point cloud completion

Dataset	CD ($\times 10^2$)				F-score (%)			
	Abutment	Pier	Pier cap	Avg.	Abutment	Pier	Pier cap	Avg.
Partial input	24.78	12.18	15.32	17.42	85.86	87.49	81.26	84.87
After completion	13.40	7.71	6.10	9.07	93.45	79.40	86.55	86.46

Table 2: Overall evaluation of dense point cloud completion

Dataset	CD ($\times 10^2$)				F-score (%)			
	Abutment	Pier	Pier cap	Avg.	Abutment	Pier	Pier cap	Avg.
Small occlusion	21.26	9.64	12.17	14.35	91.83	94.46	83.81	90.03
After completion	17.87	11.04	11.11	13.34	99.24	94.61	95.90	96.58
Large occlusion	54.68	30.38	35.11	40.05	82.33	76.29	75.87	78.16
After completion	23.63	12.00	11.72	15.78	95.46	93.02	94.44	94.30

Table 3: Evaluation of coarse point cloud completion under different occlusion conditions

Dataset	CD ($\times 10^2$)				F-score (%)			
	Abutment	Pier	Pier cap	Avg.	Abutment	Pier	Pier cap	Avg.
Small occlusion	7.41	2.21	4.67	4.76	90.39	96.31	84.97	90.55
After completion	10.39	7.37	5.77	7.84	96.12	79.91	87.97	88.00
Large occlusion	42.79	23.42	28.70	31.63	81.16	77.54	76.60	78.43
After completion	16.5	8.10	6.52	10.37	90.69	78.83	84.76	84.76

Table 4: Evaluation of dense point cloud completion under different occlusion conditions

5 CONCLUSIONS

Creating a geometric and semantically rich BIM model is critical in the Scan-to-BIM, serving as the foundation for further development of bridge DT. However, generating an accurate geometric 3D parametric model from a point cloud is still a challenging task, particularly when the point cloud suffers from serious occlusion problems. Previous bridge reconstruction methods have inevitably developed corresponding strategies to mitigate the effects of point cloud occlusion and enhance reconstruction quality. The consideration of the occlusion problem in reconstruction algorithms can impact the overall design of algorithms, resulting in poor generalizability and low robustness in the

reconstruction strategy. Addressing the point cloud occlusion can facilitate the overall reconstruction process, removing the limitation on the selection of reconstruction algorithms, enabling the successful application of algorithms and improving reconstruction accuracy.

Thus, this paper aims to advance the bridge gDT by introducing a new point cloud completion task within the current Scan-to-BIM framework, addressing point cloud occlusion as a distinct challenge. The task involves taking incomplete bridge point clouds with class labels as input and generating complete point clouds as output. To validate the proposed concept, we adopted the classical point cloud completion model PCN and validated the point cloud completion for bridge substructures, including abutments, piers, and pier caps. Both quantitative and qualitative results demonstrated a robust completion performance for point clouds with different scale occlusions.

The success of our study revealed the potential of addressing the point cloud occlusion problem after point cloud segmentation, relieving the pain in geometric reconstruction. Our study contributes to Scan-to-BIM by refining the Scan-to-BIM framework in bridge engineering. The new task point cloud completion can facilitate the bridge BIM reconstruction and the further development of DT systems. However, the occlusion in our study is generated through the spheres-based removal of point clouds, which cannot fully consider the different occlusion in real bridge data. Additionally, the application of point clouds for real-scanned bridge point clouds still needs further investigation. Thus, future work will explore the effects of different occlusion characteristics on bridge point cloud completion and the potential challenge when applying to real-scanned bridge point clouds. Training strategies for more complex bridge components, such as decks and girders, and completion performance for dense point clouds will be further explored in our future works.

ACKNOWLEDGMENTS

The authors would like to acknowledge the financial support from the University of Auckland and China Scholarship Council (Project No. 202206690016).

References

- American Society of Civil Engineers ASCE. (2021). *America's Infrastructure Report Card 2021*.
- Bosché, F. (2010). Automated recognition of 3D CAD model objects in laser scans and calculation of as-built dimensions for dimensional compliance control in construction. *Advanced Engineering Informatics*, 24(1), 107–118. <https://doi.org/10.1016/j.aei.2009.08.006>
- Bosché, F., Guillemet, A., Turkan, Y., Haas, C. T., & Haas, R. (2014). Tracking the Built Status of MEP Works: Assessing the Value of a Scan-vs-BIM System. *Journal of Computing in Civil Engineering*, 28(4), 1–13. [https://doi.org/10.1061/\(asce\)cp.1943-5487.0000343](https://doi.org/10.1061/(asce)cp.1943-5487.0000343)
- Brilakis, I. (2024). *Digital Twinning the Built Environment*. December, 17–18. <https://doi.org/10.47330/cbc.2023.mhck5583>
- Edelsbrunner, H., & Mücke, E. P. (1994). Three-Dimensional Alpha Shapes. *ACM Transactions on Graphics (TOG)*, 13(1), 43–72. <https://doi.org/10.1145/174462.156635>
- Honghong, S., Gang, Y., Haijiang, L., Tian, Z., & Annan, J. (2023). Digital twin enhanced BIM to shape full life cycle digital transformation for bridge engineering. *Automation in Construction*, 147(July 2022), 104736. <https://doi.org/10.1016/j.autcon.2022.104736>
- Huang, Z., Yu, Y., Xu, J., Ni, F., & Le, X. (2020). PF-Net: Point fractal network for 3D point cloud completion. *Proceedings of the IEEE Computer Society Conference on Computer Vision and Pattern Recognition*, 6(3), 7659–7667. <https://doi.org/10.1109/CVPR42600.2020.00768>

- Justo, A., Lamas, D., Sánchez-Rodríguez, A., Soilán, M., & Riveiro, B. (2023). Generating IFC-compliant models and structural graphs of truss bridges from dense point clouds. *Automation in Construction*, *149*(January). <https://doi.org/10.1016/j.autcon.2023.104786>
- Khudhair, A., Li, H., Ren, G., & Liu, S. (2021). Towards future BIM technology innovations: A bibliometric analysis of the literature. *Applied Sciences (Switzerland)*, *11*(3), 1–21. <https://doi.org/10.3390/app11031232>
- Liu, M., Sheng, L., Yang, S., Shao, J., & Hu, S. M. (2020). Morphing and sampling network for dense point cloud completion. *AAAI 2020 - 34th AAAI Conference on Artificial Intelligence*, 11596–11603. <https://doi.org/10.1609/aaai.v34i07.6827>
- Lu, R., & Brilakis, I. (2019). Digital twinning of existing reinforced concrete bridges from labelled point clusters. *Automation in Construction*, *105*(May), 102837. <https://doi.org/10.1016/j.autcon.2019.102837>
- Lu, R., Brilakis, I., & Middleton, C. R. (2019). Detection of Structural Components in Point Clouds of Existing RC Bridges. *Computer-Aided Civil and Infrastructure Engineering*, *34*(3), 191–212. <https://doi.org/10.1111/mice.12407>
- Mafipour, M. S., & Vilgertshofer, S. (2023). Automated geometric digital twinning of bridges from segmented point clouds by parametric prototype models. *Automation in Construction*, *156*(May). <https://doi.org/10.1016/j.autcon.2023.105101>
- Mehranfar, M., Arefi, H., & Alidoost, F. (2021). Knowledge-based 3D reconstruction of bridge structures using UAV-based photogrammetric point cloud. *Journal of Applied Remote Sensing*, *15*(04), 1–26. <https://doi.org/10.1117/1.jrs.15.044503>
- Pregolato, M., Gunner, S., Voyagaki, E., De Risi, R., Carhart, N., Gavriel, G., Tully, P., Tryfonas, T., Macdonald, J., & Taylor, C. (2022). Towards Civil Engineering 4.0: Concept, workflow and application of Digital Twins for existing infrastructure. *Automation in Construction*, *141*(July), 104421. <https://doi.org/10.1016/j.autcon.2022.104421>
- Preparata, F. P., & Hong, S. J. (1977). Convex Hulls of Finite Sets of Points in Two and Three Dimensions. *Communications of the ACM*, *20*(2), 87–93. <https://doi.org/10.1145/359423.359430>
- Schönfelder, P., Aziz, A., Faltin, B., & König, M. (2023). Automating the retrospective generation of As-is BIM models using machine learning. *Automation in Construction*, *152*, 104937. <https://doi.org/10.1016/j.autcon.2023.104937>
- Tchapmi, L. P., Kosaraju, V., Rezatofighi, H., Reid, I., & Savarese, S. (2019). Topnet: Structural point cloud decoder. *Proceedings of the IEEE Computer Society Conference on Computer Vision and Pattern Recognition*, *2019-June*, 383–392. <https://doi.org/10.1109/CVPR.2019.00047>
- Walsh, S. B., Borello, D. J., Guldur, B., & Hajjar, J. F. (2013). Data processing of point clouds for object detection for structural engineering applications. *Computer-Aided Civil and Infrastructure Engineering*, *28*(7), 495–508. <https://doi.org/10.1111/mice.12016>
- Wang, X., Ang, M. H., & Lee, G. H. (2022). Cascaded Refinement Network for Point Cloud Completion With Self-Supervision. *IEEE Transactions on Pattern Analysis and Machine Intelligence*, *44*(11), 8139–8150. <https://doi.org/10.1109/TPAMI.2021.3108410>
- Wen, X., Li, T., Han, Z., & Liu, Y. S. (2020). Point Cloud Completion by Skip-Attention Network with Hierarchical Folding. *Proceedings of the IEEE Computer Society Conference on Computer Vision and Pattern Recognition*, 1936–1945. <https://doi.org/10.1109/CVPR42600.2020.00201>
- Yan, Y., & Hajjar, J. F. (2022). Geometric models from laser scanning data for superstructure components of steel girder bridges. *Automation in Construction*, *142*. <https://doi.org/10.1016/j.autcon.2022.104484>
- Yang, T., Zou, Y., Yang, X., & del Rey Castillo, E. (2024). Domain knowledge-enhanced region growing framework for semantic segmentation of bridge point clouds. *Automation in Construction*, *165*(November 2023), 105572. <https://doi.org/10.1016/j.autcon.2024.105572>

- Yi, L., Kim, V. G., Ceylan, D., Shen, I. C., Yan, M., Su, H., Lu, C., Huang, Q., Sheffer, A., & Guibas, L. (2016). A scalable active framework for region annotation in 3D shape collections. *ACM Transactions on Graphics*, 35(6), 1–12. <https://doi.org/10.1145/2980179.2980238>
- Yuan, W., Khot, T., Held, D., Mertz, C., & Hebert, M. (2018). PCN: Point completion network. *Proceedings - 2018 International Conference on 3D Vision, 3DV 2018*, 728–737. <https://doi.org/10.1109/3DV.2018.00088>
- Zhao, B., Chen, X., Hua, X., Xuan, W., & Lichti, D. D. (2023). Completing point clouds using structural constraints for large-scale points absence in 3D building reconstruction. *ISPRS Journal of Photogrammetry and Remote Sensing*, 204(September), 163–183. <https://doi.org/10.1016/j.isprsjprs.2023.09.008>
- Zhuang, Z., Zhi, Z., Han, T., Chen, Y., Chen, J., Wang, C., Cheng, M., Zhang, X., Qin, N., & Ma, L. (2024). A Survey of Point Cloud Completion. *IEEE Journal of Selected Topics in Applied Earth Observations and Remote Sensing*, 17, 1–22. <https://doi.org/10.1109/jstars.2024.3362476>